

Vibrational layer eigenmodes of binary phospholipid-cholesterol bilayers at low temperaturesD. V. Leonov,¹ S. V. Adichtchev,² S. A. Dzuba,^{1,3} and N. V. Surovtsev^{1,2,*}¹*Department of Physics, Novosibirsk State University, Novosibirsk 630090, Russia*²*Institute of Automation and Electrometry, Russian Academy of Sciences, Novosibirsk 630090, Russia*³*Institute of Chemical Kinetics and Combustion, Russian Academy of Sciences, Novosibirsk 630090, Russia*

(Received 18 October 2018; revised manuscript received 11 January 2019; published 22 February 2019)

Raman spectra in the low-frequency spectral range—between 5 and 90 cm^{-1} —were studied for multilamellar bilayers prepared with cholesterol (Chol) and phospholipids of three different types: doubly unsaturated lipids 1,2-dioleoyl-sn-glycero-3-phosphocholine (DOPC), monounsaturated lipids 1-palmitoyl-2-oleoyl-sn-glycero-3-phosphocholine (POPC), and fully saturated lipids 1,2-dimyristoyl-sn-glycero-3-phosphocholine (DMPC). The narrow peak seen below 250 K and positioned between 9 and 18 cm^{-1} —depending on the system and temperature—was attributed to the vibrational eigenmode of a lipid monolayer. For the DOPC-Chol bilayer, the peak position and the peak width were found to monotonically increase and decrease, respectively, with the Chol concentration. For POPC-Chol and DMPC-Chol bilayers, these parameters revealed nonmonotonic concentration dependences, with an apparent minimum at the intermediate Chol content. The peak intensity was ascribed to interleaflet coupling. As in the literature, a coexistence of liquid-ordered and solid-ordered domains was suggested for the DMPC-Chol and POPC-Chol bilayers; the Chol concentration dependences of Raman peak parameters were discussed in line with this suggestion, under the assumption that the different composition of coexisting domains conserves upon cooling. We demonstrated that the obtained Raman data disagree with the suggested domain coexistence if the domain sizes are substantially larger than the lipid layer thickness.

DOI: [10.1103/PhysRevE.99.022417](https://doi.org/10.1103/PhysRevE.99.022417)**I. INTRODUCTION**

Phospholipids are the main component of plasma membranes, which also includes other lipids, cholesterol (Chol), membrane proteins, fatty acids, and other components. To model various membrane properties, artificial bilayers made of synthetic lipids and Chol are often used [1]. One of the most interesting properties of Chol-containing multicomponent membranes is their ability to have two-phase coexistence, where domains of the so-called liquid-ordered phase (L_o , ordered hydrocarbon chains, which exhibit high lateral and rotational mobility) coexist with domains of a liquid-disordered (L_d , fluid) phase or solid-ordered (S_o , gel) phase [2,3]. The L_o domains attract attention in relation to the lipid raft concept, which is considered as an important factor for various cellular processes [4–6]. The two-phase coexistence in lipid layers is studied by different approaches, such as fluorescence microscopy [7–10], nuclear magnetic resonance (NMR) [11,12], spin-label electron spin resonance (ESR) spectroscopy [3,13], computer simulations [14,15], and others. However, the nature of two-phase coexistence has remained obscure [16–22]. Moreover, for binary lipid-Chol mixtures, there is no consensus attained on the two-phase coexistence [23,24]. Thus, the development of new experimental approaches to get information on the nanoscale lateral structure of multicomponent phospholipids bilayers remains a challenging task.

Here, we study the capability of a low-frequency Raman scattering technique for the description of properties of binary bilayers. Recently [25], it was shown that the Raman spectrum of multilamellar phospholipid bilayers in the frequency range between 5 and 90 cm^{-1} at low temperatures (<270 K) contains two peaks: one located near 8–9 cm^{-1} and ascribed to the first vibrational eigenmode of the bilayer, and another located near 14–17 cm^{-1} and ascribed to the first vibrational eigenmode of a single monolayer (a leaflet). These peaks are not observed in the fluid phase or above 270 K for hydrated samples, and this is attributed to mode overdamping by fast relaxational motions. Since the coexisting domains of different phases in Chol-containing membranes must be of different Chol composition, cooling to low temperatures should also lead to the coexisting frozen domains of different compositions. Since bilayer composition determines the membrane thickness and elastic modulus, this may affect the eigenmode frequencies. Average bilayer composition is reflected in the position of the layer eigenmode Raman peaks, while the composition fluctuations influence the inhomogeneous linewidth.

In the present work, the low-frequency Raman scattering is studied for three binary phospholipids-Chol mixtures containing doubly unsaturated lipids 1,2-dioleoyl-sn-glycero-3-phosphocholine (DOPC), monounsaturated lipids 1-palmitoyl-2-oleoyl-sn-glycero-3-phosphocholine (POPC), or fully saturated lipids 1,2-dimyristoyl-sn-glycero-3-phosphocholine (DMPC). Some works (e.g., [2,26,27]) report on the two-phase coexistence in mixtures of Chol with DMPC or POPC. We are not aware of reports confirming the two-phase coexistence for the mixture of Chol and DOPC. The parameters of the low-frequency Raman peaks

*Corresponding author: lab21@iae.nsk.su

obtained here are discussed in line with the expectations for a heterogeneous versus homogeneous scenario of the lateral organization in lipid layers.

II. MATERIALS AND METHODS

A. Sample preparation

Phospholipids DOPC, POPC, and DMPC were purchased from Avanti Polar Lipids, and Chol was purchased from Sigma Aldrich; these substances were used without further purification. Phospholipids and Chol taken at different compositions (up to the Chol molar fraction equal to 0.5 of the dry mixture) were mixed, dissolved in chloroform, and then subjected to overnight evaporation under vacuum. The obtained compositions were dispersed in water (lipid-to-water ratio of 1:1.5 w/w) by heating above the gel-to-fluid phase transition with vortex mixing at $T = 26^\circ\text{C}$. Then these samples were subjected to a few freezing-thawing cycles. This protocol leads to the aqueous suspensions of spherical multilamellar bilayers with typical diameters in the range between 1 and 3 microns. These suspensions were placed in glass tubes of 3 mm outer diameter and sealed.

B. Raman experiment

The low-frequency Raman spectra of aqueous phospholipid suspensions were recorded by the use of a triple-grating TriVista 777 spectrometer and a 532 nm laser (Millenia, Spectra Physics). Measurement of the low-frequency Raman spectrum from an opaque white sample such as the phospholipid suspension is a demanding task since there is a need to have a very high contrast of the instrumental response for the low-frequency Raman shift. Spurious background of the laser beam was suppressed by a monochromator described in [28]. The laser beam of 50 mW power was focused into the sample by a lens of 60 mm focal length and the light scattered at the right angle was collected by a lens with a focal length of 60 mm. The spectrum of a neon-discharge lamp was used for the wavelength calibration of the spectrometer.

Raman spectra in three spectral ranges (from -230 to -5 cm^{-1} , from 15 to 495 cm^{-1} , and from 283 to 800 cm^{-1}) were acquired. The spectral ranges from 15 to 495 cm^{-1} and from 285 to 800 cm^{-1} were measured with two gratings of 900 grooves/mm operating in the subtractive mode and the third grating of 1800 grooves/mm responsible for the spectral resolution. The spectral range from -230 to -5 cm^{-1} was measured with two gratings of 1800 grooves/mm operating in the subtractive mode and the third grating of 1800 grooves/mm responsible for the spectral resolution. The entrance slit was $100\text{ }\mu\text{m}$ for the spectral ranges from 15 to 495 cm^{-1} and from 283 to 800 cm^{-1} (2 cm^{-1} of the FWHM spectral resolution). For the spectral range from 283 to 800 cm^{-1} , the slit before the last monochromator was $380\text{ }\mu\text{m}$. For the spectral range from 15 to 495 cm^{-1} , the slit before the last monochromator was as low as $150\text{ }\mu\text{m}$ in order to improve the instrumental contrast for the low-frequency Raman shift. In this case, a spectral distortion of the light transmission should be taken into account for the used spectrometer. This correction was made by the comparison with the spectrum measured with the $380\text{ }\mu\text{m}$ slit before the last monochromator.

The slit after the first monochromator determines the spectral range of the measurement. For the Raman experiment with the spectral range from 283 to 800 cm^{-1} , the slit was fully open ($12\,000\text{ }\mu\text{m}$), corresponding to the acquisition of the whole spectral range. For acquisition below 495 cm^{-1} , the slit was adjusted to suppress the elastic line penetration into the third monochromator. Nevertheless, even for very strong suppression of the elastic line, the spectra contained a spurious contribution below 15 cm^{-1} of the Raman shift. Spurious origin of this contribution was proved by measuring the elastic scattering from a metal surface. Presumably, this is unsuppressed sidebands of the laser outcome. Thus, by using the Stokes side of the spectrum, we were able to get the Raman spectra being free from the elastic line or spurious contribution down to 15 cm^{-1} . The spectra measured in the range from 15 to 495 cm^{-1} and from 283 to 800 cm^{-1} were combined into a total spectrum ranging from 15 to 800 cm^{-1} .

To acquire Raman lines at lower frequencies, we performed measurements in the anti-Stokes side of the spectrum, which is free from the spurious contributions in our setup [29]. In these measurements, all three gratings were of 1800 grooves/mm, to improve the elastic line suppression. With these gratings, the acquired spectral range was about 250 cm^{-1} . The entrance slit was $50\text{ }\mu\text{m}$ (1 cm^{-1} of the FWHM spectral resolution), and the slit before the last monochromator was $150\text{ }\mu\text{m}$. The correction for the spectrometer transmission was made as described above. The slit after the first monochromator was adjusted to suppress the elastic line penetration into the third monochromator. The observed lack of the anomalous temperature dependence of the Bose-scaled spectra proved that the spectra are free from the elastic scattering contribution down to 5 cm^{-1} . Indeed, the elastic scattering contribution is temperature independent, while absolute Raman intensity at low frequencies is proportional to temperature, so the elastic line contribution to the spectra is manifested as an apparent increase of the Bose-scaled spectra at low frequencies as the temperature decreases. After correction to the Stokes-to-anti-Stokes ratio, this anti-Stokes spectrum was used to extend the Raman spectrum measured in the Stokes side to lower frequencies. Finally, we got the Raman spectrum from 5 to 800 cm^{-1} for the samples studied.

An optical closed-cycle helium cryostat of Advanced Research Systems was used to provide the Raman experiment at different temperatures. The cooling protocol includes the sample cooling from room temperature down to 100 K with a cooling rate of 3 K/min, which was followed by heating to the desired temperature of the experiment. The experimental spectra comprised a photoluminescence contribution, which was the highest at 100 K and by a few times lower at 240 K. The photoluminescence background was subtracted from the measured spectra using a cubic polynomial approximation in the spectral range between 5 and 800 cm^{-1} .

III. RESULTS

In Fig. 1, the obtained experimental Raman spectra $I(\nu)$ taken between 100 and 240 K for DOPC bilayers are shown. The spectra were converted into the spectral density

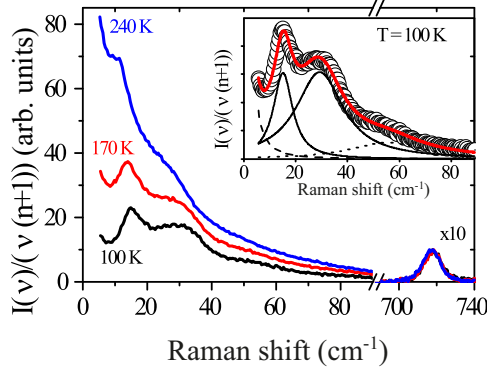


FIG. 1. Low-frequency Raman spectra for DOPC bilayers at 100, 170, and 240 K. In the inset, the experimental spectrum at $T = 100$ K is presented via circles, and the thick solid line is its approximation with a sum of four Lorentzians (the dashed, dotted, and two thin lines).

representation,

$$I_n(\nu) = \frac{I(\nu)}{\nu[n(\nu, T) + 1]}, \quad (1)$$

where $n(\nu, T)$ is the Bose factor. In this presentation, the vibrational spectrum is temperature independent in the harmonic approximation. Also, the spectra were scaled by the Raman intensity of the C–N mode (near 720 cm^{-1}), which is known to be temperature independent [30].

One can see in Fig. 1 three peaks: near 15 , 30 , and $50\text{--}60 \text{ cm}^{-1}$. According to the previous analysis [25], the peak position ν_m near 15 cm^{-1} may be attributed to the first eigenmode of the lipid monolayer,

$$\nu_m = \frac{u}{2cd}, \quad (2)$$

where c is the light speed, u is the velocity of sound propagating in the normal direction to the lipid bilayers, and d is the monolayer thickness. Equation (2) provides the lowest eigenmode frequency of a thick plate of thickness d in the continuum approximation. For the bilayer thickness $2d$ taken as $\sim 5 \text{ nm}$ and velocity $u \sim 1.64 \text{ km/s}$ (the value found for the room-temperature velocity of the longitudinal sound propagating along the normal of the lipid bilayer in the case of almost dry phospholipids [31]), Eq. (2) provides an estimation $\nu_m \approx 11 \text{ cm}^{-1}$. This is the reason for the attribution of the 15 cm^{-1} peak to the first eigenmode of the lipid monolayer (at $T = 240 \text{ K}$, according to data in Fig. 1, $\nu_m \approx 11.5 \text{ cm}^{-1}$). Note that the first eigenmode of the lipid bilayer should be at the frequency that is twice lower than that for the first eigenmode of the lipid monolayer.

The origin of the mode near 30 cm^{-1} in Fig. 1 is less clear. Previously [25], this mode was attributed to the third eigenmode of the bilayer. But for the DOPC bilayer (see Fig. 1), its apparent position is close to the second eigenmode of the monolayer, which is forbidden for Raman scattering. The bump seen in Fig. 1 in the $50\text{--}60 \text{ cm}^{-1}$ range may be attributed to the contribution from acousticlike excitations spreading in the lateral direction [25]. A peak with the center at zero frequency (central peak) increases with temperature faster than the Bose factor and may be tentatively explained as relaxation

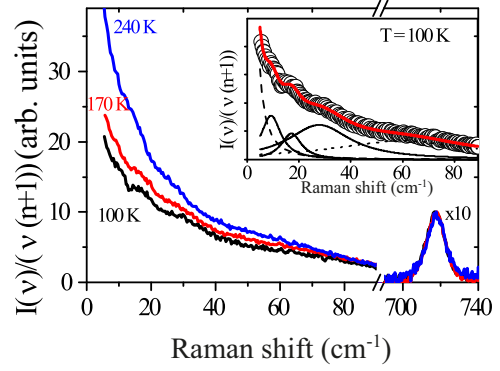


FIG. 2. The same as in Fig. 1, for the DMPC bilayers.

contribution. Contributions from 30 cm^{-1} , $50\text{--}60 \text{ cm}^{-1}$, and central modes are taken into account in the Raman spectrum description, but they are not the goal of the present work.

To extract the low-frequency peak parameters from the experimental Raman spectra, the spectra were fitted by a sum of four Lorentzians, one of which is the central peak—see the inset to Fig. 1. One can see that this description works well.

For the cholesterol-free POPC bilayers, the low-frequency $I_n(\nu)$ spectra were presented in [25]. (Raman spectra for cholesterol-free POPC and 1:1 POPC:Chol bilayers reported in [25] were similar to those found in the present work.)

Figure 2 shows $I_n(\nu)$ spectra obtained for the DMPC bilayers. One can see that the eigenmode peaks are less pronounced here, looking like merely spectral shoulders. In contrast with the DOPC data (cf. Fig. 1), a contribution of the bilayer eigenmode [25] (the peak near 9.2 cm^{-1}) is seen; the other layer modes are seen near 17.1 and 27.8 cm^{-1} .

Note that the low-frequency Raman spectra allow checking the Chol incorporation into the bilayer. The data in Fig. 3 show that the Raman spectrum for pure Chol has peculiar lines, belonging to the crystalline lattice modes, and the mechanical POPC-Chol 1:1 mixture (prepared with dispersing

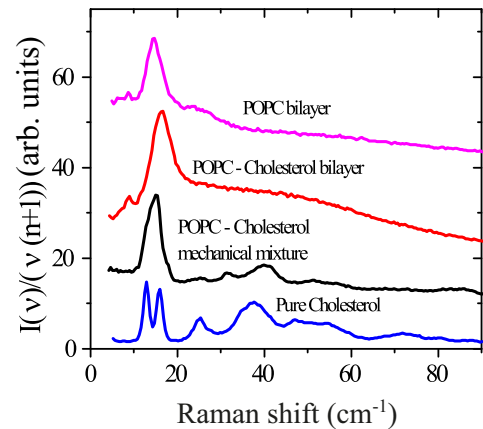


FIG. 3. Low-frequency Raman spectra at 100 K for crystalline Chol, POPC and POPC-Chol (1:1) bilayers obtained with the protocol described in Sec. II A, and the aqueous suspensions of the POPC-Chol mixture (1:1) prepared without preceding dissolution in chloroform (mechanical mixture). Spectra are shifted upwards for convenience.

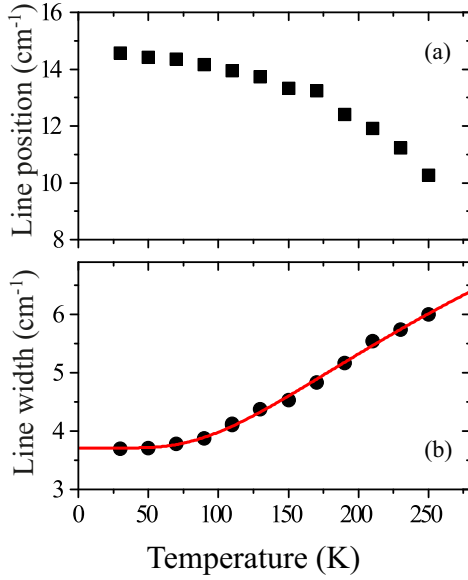


FIG. 4. Temperature dependence of (a) peak position and (b) width for the Raman monolayer eigenmode peak in POPC-Chol bilayers (6.3 mol% of Chol). The line drawn through the points is a fit employing Eq. (3).

in water but without the intermediate stage of dissolution in chloroform) exhibits these lines as well. At the same time, the protocol described in Sec. II A results in the disappearance of crystalline Chol lines. This proves that Chol molecules are well dissolved in our samples.

The detailed temperature dependence for the monolayer eigenmode peak position and width obtained for the POPC-Chol bilayers (with 6.3 mol% Chol content) are given in Fig. 4. The data were obtained from the experimental spectra by Lorentzian deconvolution, as was shown in Figs. 1 and 2. It is seen in Fig. 4 that the peak position is descending with the temperature increase, and that the peak becomes broader.

The decrease of the peak position with temperature in Fig. 4 may be explained by anharmonic effects, which become more pronounced with temperature, and also by decrease of the sound velocity. The increase of the peak width means that, except for the inhomogeneous broadening caused by fluctuation of the elastic modulus which is temperature independent, the homogeneous broadening is also important. The homogeneous broadening corresponds to shortening the vibration lifetime, which is expected with the temperature increase.

Figure 4 also shows that the peak width of the Raman peak $\gamma(T)$ may be described by the relation

$$\gamma(T) = \gamma_0 + Ae^{-U/T}, \quad (3)$$

where γ_0 is the inhomogeneous broadening, U is the effective barrier responsible for the vibration decay, and A is a constant. Equation (3) describes well the experimental peak width, with the best-fitted parameter $U = 356 \pm 14$ K. Interestingly, this U value corresponds well to the energy difference between *trans* and *gauche* conformations [32].

Figure 5 shows the representative low-frequency Raman spectra for DOPC-Chol, DMPC-Chol, and POPC-Chol bilay-

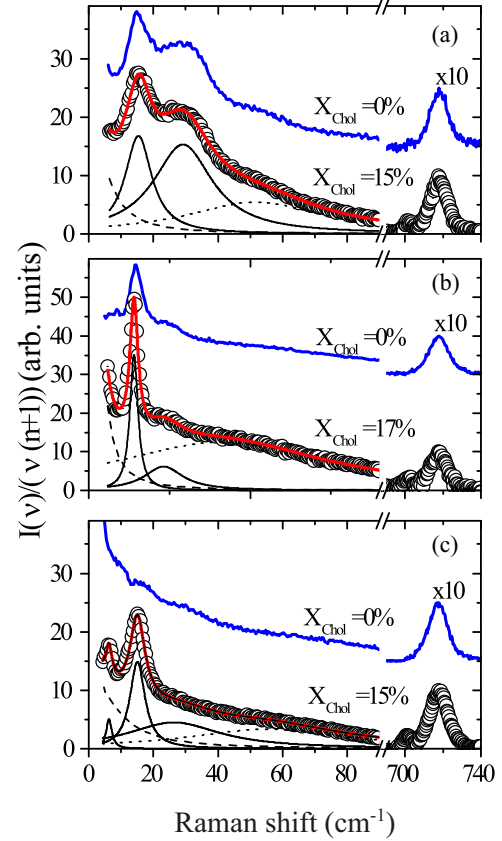


FIG. 5. Representative Raman spectra for (a) DOPC-Chol (15 mol% of Chol), (b) POPC-Chol (17 mol% of Chol), and (c) DMPC-Chol (15 mol% of Chol) bilayers obtained at $T = 100$ K (empty circles). Spectra are deconvoluted into a sum of four Lorentzians (thick lines drawn through the circles). The dashed line corresponds to the central peak contribution, the thin solid lines correspond to the phospholipid layer modes, and the dotted line reflects a contribution from the acousticlike excitations. The spectra of the Chol-free samples are shown for comparison (shifted upward for convenience).

ers. One can see that for the Chol-free DMPC bilayers, the monolayer eigenmode peak near 15 cm^{-1} has low intensity and that Chol addition leads to its significant increase. In the case of unsaturated DOPC and POPC phospholipids, the Chol effect is manifested only in the Raman peak positions and widths. Also, a new Raman mode appears near 700 cm^{-1} with Chol addition (Fig. 5). This mode is ascribed to the Chol internal vibration; it may be used to control the Chol incorporation into the bilayer.

Low-frequency Raman spectra for the DOPC-Chol, POPC-Chol, and DMPC-Chol bilayers were deconvoluted into a sum of Lorentzians; see Fig. 5. The parameters of the Lorentzians for the monolayer eigenmode Raman peak were extracted for all temperatures studied. The Chol concentration dependences of the monolayer eigenmode peak position and width are shown in Figs. 6, 7, and 8 for the DOPC-Chol, POPC-Chol, and DMPC-Chol bilayers, respectively.

One can see that in the case of DOPC (Fig. 6), both the peak position and width demonstrate simple monotonic behaviors as the Chol concentration increases. However, in

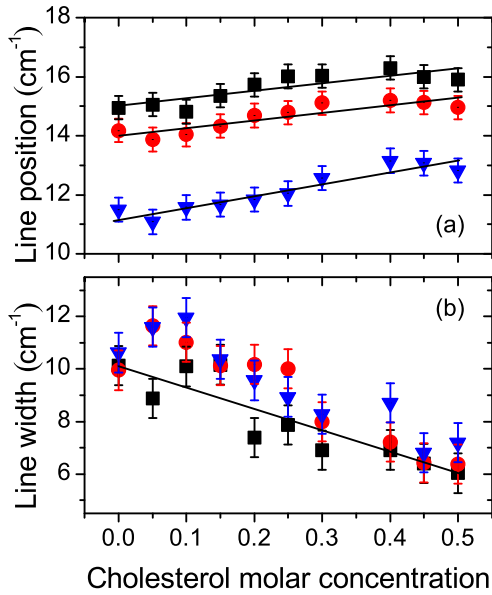


FIG. 6. The (a) peak position and (b) width vs Chol concentration for the DOPC-Chol bilayers taken at 100 K (black squares), 170 K (red circles), and 240 K (blue triangles). The solid lines present the linear description of the data.

the cases of POPC (Fig. 7) and DMPC (Fig. 8), the behavior is nonmonotonic, with the decrease at low ($< \sim 10$ mol%) Chol concentration, attaining a minimum at the intermediate concentration range, and with an increase at high concentrations.

For the POPC bilayers (Fig. 7), three temperature ranges are seen in Fig. 7(b), which are highlighted by the straight-line

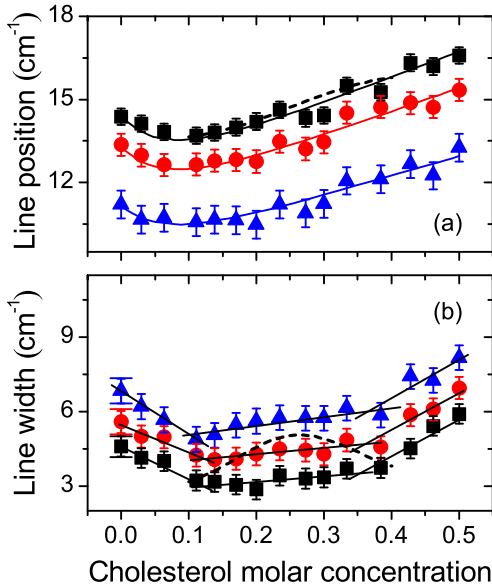


FIG. 7. The same as in Fig. 6, for the POPC-Chol bilayers. In (a), the solid lines describe the concentration dependence of the peak position given by Eq. (5). In (b), three straight-line segments reveal ranges with different behavior of the peak width. The dashed lines in (a) and (b) are expectations for the peak position and width at 100 K, in the case of the two-phase coexistence in the range from 10 to 40 mol% of Chol content (see text for details).

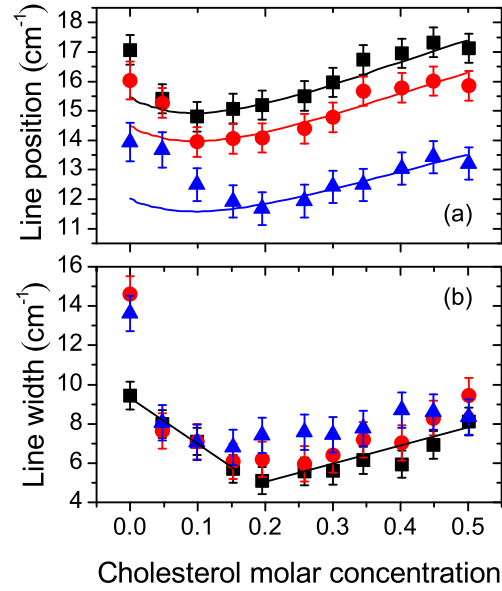


FIG. 8. The same as in Fig. 7, for DMPC-Chol bilayer. In (b), two straight-line segments reveal ranges with different behavior of the peak width.

segments. The boundaries between the ranges occur near 10 and 35 mol% Chol concentration.

For the case of DMPC-Chol bilayers (Fig. 8), the Chol effect is qualitatively similar to the case of POPC-Chol bilayers (cf. Fig. 7). Quantitatively, the difference between these two systems is the significantly higher width for pure DMPC and its sharper decrease in the concentration range below 10 mol%. Note that data fitting for the cholesterol-free DMPC bilayer is less unambiguous since the layer peak here is less prominent (Fig. 2), which is in contrast to the case of Chol-containing DMPC bilayers [Fig. 5(c)]. This leads to some uncertainties of fitting parameters found for the spectra at 170 and 240 K for the cholesterol-free DMPC sample. The rest of the data demonstrate a decrease of the peak width towards the Chol concentration near 10–20 mol% and a next moderate increase.

As Fig. 5(c) reveals some increase of the Raman intensity of the monolayer eigenmode with Chol addition to DMPC, this effect was studied as a function of Chol concentration. The data are presented in Fig. 9, along with results for two other phospholipid-Chol bilayers (only data obtained at $T = 100$ and 170 K are shown because at $T = 240$ K the data show significant scattering). It is seen that in the case of DMPC, the Chol addition leads to an approximately 3.5-fold increase of the Raman peak intensity so that the dependence has a steplike behavior in the range from 10 to 20 mol%. For the POPC-Chol bilayer, the increase also takes place but here it is weaker and has a smoothed behavior. In the case of the DOPC-Chol bilayer, no Chol-induced increase of the Raman intensity of the monolayer eigenmode is observed.

IV. DISCUSSION

The found Chol concentration dependence for the peak position ν_m is nonmonotonic for POPC-Chol and DMPC-Chol bilayers, as seen in Figs. 7 and 8. The ν_m value, according to

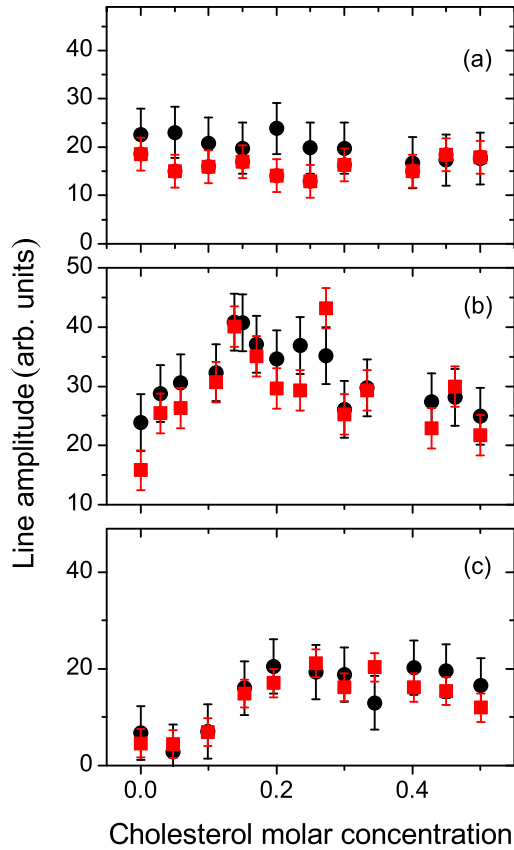


FIG. 9. The Raman monolayer eigenmode intensity vs Chol concentration for the (a) DOPC-Chol, (b) POPC-Chol, and (c) DMPC-Chol bilayers. Temperature is 100 K (red squares) and 170 K (black circles).

Eq. (2), is defined by the ratio of the sound velocity u and the layer thickness d . Therefore, the dependence could be explained taking into account the possible Chol influence on the longitudinal acoustic velocity u and the layer thickness d . One may expect that the addition of Chol, which is a rigid molecule, leads to a d increase through decreasing the tilt angle [33]; at least it is expected in the case of the saturated phospholipids which are prone to the significant tilt slope. The sound velocity u is also expected to increase due to the higher rigidity of Chol in comparison with phospholipids. Unfortunately, no data are available in the literature for the u values in these phospholipid-Chol bilayers, to the best of our knowledge. We suggest that u can be approximated by a linear dependence,

$$u = u_0(1 + \alpha X_{\text{Chol}}), \quad (4)$$

where u_0 is the sound velocity for Chol-free lipid layers, X_{Chol} is the Chol molar concentration, and α is a fitting parameter. Combining Eqs. (2) and (4), the experimental peak position is described by the relation

$$v_m = \frac{u_0(1 + \alpha X_{\text{Chol}})}{2cd}, \quad (5)$$

with two fitting parameters (u_0 and α). We used x-ray data for the POPC-Chol and DMPC-Chol bilayers reported on the bilayers thickness d at room temperature [34]. Under the

assumption that Chol affects the layer thickness in a similar way for the fluid and frozen state, we applied Eq. (5) to describe our data. The results are shown in Figs. 7(a) and 8(a). One can see that this description works satisfactorily well for POPC-Chol bilayers [Fig. 7(a)]. In the case of DMPC-Chol bilayers [Fig. 8(a)], this description catches the trend, but it underestimates the line position at low Chol concentration. Probably, this quantitative difference can be attributed to a difference of Chol effect on the phospholipid thickness at room and low temperatures. In general, the nonmonotonic dependence of the layer mode frequency reflects the interplay between the Chol influence on the layer thickness and the sound velocities. [Since this interpretation employs the high-temperature data for $d(X_{\text{Chol}})$, no quantitative outcomes can be done from this description.]

In contrast to the DMPC-Chol and POPC-Chol bilayers, the $v_m(X_{\text{Chol}})$ dependence in the DOPC-Chol bilayer shows a monotonic behavior; see Fig. 6(a). Probably this is related to the lower Chol effect on the tilt angle in the case of DOPC. Data for $d(X_{\text{Chol}})$ dependence at low temperatures, lacking at present, would clarify the situation.

In the cases of POPC-Chol and DMPC-Chol bilayers, the peak width decreases at low Chol concentration (< 10 mol%); see Figs. 7(b) and 8(b). In the case of the DOPC-Chol bilayer, the peak width decreases in the entire Chol concentration range [Fig. 6(b)]. Since for different temperatures it looks similar [Figs. 6(b), 7(b), 8(b)], the peak width decrease is related to changes in inhomogeneous peak broadening. This raises the question of how the inhomogeneous width in the Chol-free sample can be wider than for the binary systems. Probably this effect may be attributed to a tendency of a monocomponent bilayer to form a crystallinelike order for the lateral molecular positions in the bilayer [35,36]. Then, small lateral crystallinelike domains serve as lateral inhomogeneities, which should result in an inhomogeneous width increase. In addition, a ripplelike crystalline state of monocomponent bilayer [37] can also increase the inhomogeneous width. We cannot judge which mechanism prevails, but both reasons can attribute the observed additional inhomogeneous peak broadening to the crystallinelike lateral domains. It may be assumed that the Chol addition either inhibits the growth of the crystallinelike lateral domains or sticks them together, making the bilayer structure more homogeneous.

In the cases of POPC-Chol and DMPC-Chol bilayers, a minimum of the peak width is achieved near Chol concentration of 10–20 mol%, which might be ascribed to the complete suppression of the separate crystallinelike lateral domains. Probably, in the case of a DOPC-Chol sample, a higher Chol concentration is needed for this suppression, when Chol only weakly disturbs the DOPC bilayer lateral structure, by filling mainly free-volume-like places. This interpretation is in line with a weaker Chol effect on the tilt angle in DOPC, assumed above to explain the monotonic dependence of $v_m(X_{\text{Chol}})$. The remarkable increase of the peak width above ~ 40 mol% Chol content observed for the POPC-Chol bilayer [Fig. 7(b)] and the moderate increase above ~ 20 mol% Chol content observed for the DMPC-Chol bilayer [Fig. 8(b)] may be interpreted as an oversaturation effect in the Chol addition.

For the DMPC-Chol and POPC-Chol bilayers, there are suggestions in the literature [23] on the two-phase

coexistence for some concentration ranges (at room temperature). The coexisting domains must have the different lipid-Chol compositions, and one may suggest that upon cooling, these domains of different compositions are captured. Then these domains are expected to be manifested in the low-temperature low-frequency Raman spectra studied here.

We can compare our low-frequency Raman data with these expectations. For the case when the assumed domains of different phases and compositions are significantly larger than the layer thickness (2–3 nanometers), this assumption drives the low-temperature domains to vibrate separately (independently). For the DMPC-Chol bilayer, two-phase diagrams were proposed for coexisting phases. First, in [26], the coexisting S_o and L_o phases were suggested to exist in the range from 6 to 30 mol%; below and above this range only one phase is present—either S_o or L_o , respectively. Second, in [38], the coexisting S_o and L_o phases were detected in the range below 21 mol%; above this threshold, only the L_o phase exists. The coexistence range implies that for a given DMPC-Chol composition within this range, the domains are expected to be of two compositions corresponding to the low- or high-concentration edges [2]. In this case, the peak position is a linear combination of the positions for the low-Chol and high-Chol concentrations and cannot achieve minimum within the coexistence range. It is seen that Fig. 8(a) contradicts this expectation for the phase diagram of [38] (minimum is near 10 mol% for the data at $T = 100$ K). Note that the markedly nonlinear concentration dependence for the monolayer peak Raman intensity in the range 0–20 mol% [Fig. 9(c)] is also against the coexisting separate phases in this range. Similar arguments (the peak position minimum and the nonlinear concentration dependence for the monolayer peak Raman intensity) also evidence against the coexisting separate phases in the range from 6 to 30 mol%.

In the case of the POPC-Chol system, phase diagrams with coexisting phases were also suggested [23]. In some of them, the coexisting S_o and L_o phases were proposed below ~ 20 mol% [39]. Again, the minimum near 10 mol% [Fig. 7(a)] contradicts this suggestion. Another case is the phase diagram with coexisting S_o and L_o phases depicted in the range from 10 to 40 mol% [27]. Here, below and above this range, only one phase is present (either S_o or L_o , respectively). In this case, the peak position and width versus Chol concentration can be predicted since we know spectral shapes of the peaks at the edges of the assumed coexistence range. In this case, the Raman peak for an intermediate Chol concentration is the sum of these peaks, weighted by the content of the S_o and L_o phases. Applying the lever rule [2] in the determination of the component contributions from the phase diagram, we can simulate the peak at an intermediate Chol concentration and evaluate its position and width from a Lorentzian fit. Results are shown in Fig. 7. One can see that this expectation for the peak width contradicts the two-composition coexistence in the range from 10 to 40 mol%. Note that a maximum of the peak width is expected within the assumed two-composition range for any case, when the peak position monotonically increases with the Chol concentration. Thus, the data of Figs. 7 and 8 do not support any two-composition coexistence with edges within 10 to 50 mol% for DMPC-Chol and POPC-Chol systems.

The above analysis is done with the assumption that the two-composition range of two S_o phases at low temperatures is the same as the S_o - L_o coexistence range at high temperatures. Note that if during cooling there is no partial dissolving of the solid phase or changes in the S_o composition, the border between the S_o - L_o and L_o ranges can shift only to a higher Chol concentration, corresponding to the higher Raman peak position [Fig. 7(a)]. In this case, the disagreement between the peak width, calculated for two-phase coexistence, and the experimental data remains. Thus, for DMPC-Chol and POPC-Chol bilayers, the low-frequency Raman data contradict the possibility of the coexistence of different composition domains whose sizes are significantly larger than the bilayer thickness.

As it was indicated in [25], the monolayer eigenmode is forbidden for the Raman scattering when there is a good elastic coupling between two leaflets of the phospholipid bilayer. Decoupling between the leaflets removes this forbidding, and the monolayer eigenmode can be observed in the Raman experiment. Therefore, the Raman intensities of the monolayer eigenmode can serve as a measure of the elastic coupling between leaflets. The data shown in Fig. 9 present an example of how the Raman intensity is employed to measure the interleaflet coupling (with spectra scaling by a Raman mode near 720 cm^{-1}). These data reveal that the interleaflet coupling is low for the unsaturated (POPC, DOPC) phospholipids, and the Chol addition does not significantly change the Raman intensity of the monolayer eigenmode. In contrast, the interleaflet coupling is much stronger for the saturated (DMPC) phospholipids and the Chol addition reduces this coupling, thereby significantly increasing the Raman intensity of the monolayer eigenmode.

V. CONCLUSIONS

Low-frequency Raman spectroscopy (in the frequency range between 5 and 90 cm^{-1}) was applied to phospholipid-Chol bilayers, with phospholipids been either doubly unsaturated DOPC, monounsaturated POPC, or fully saturated DMPC. Low-temperature Raman spectra contain several peaks interpreted as vibrational eigenmodes of a lipid monolayer (a leaflet) or of a lipid bilayer. The deconvolution of the experimental spectra into a sum of several Lorentzians allows one to separate these peaks. The most narrow and well-defined peak is located, depending on the system and temperature, between 9 and 18 cm^{-1} . This peak was attributed to a vibrational eigenmode of the lipid monolayer. Its width, position, and intensity were studied in detail as a function of Chol concentration.

The Chol concentration dependences of the monolayer eigenmode width and position were discussed in relation to the possible two-phase coexistence suggested in the literature for POPC-Chol and DMPC-Chol bilayers. For these systems, the monolayer peak position and width were found to show nonmonotonic concentration dependences, with an apparent minimum at an intermediate Chol concentration range. The concentration dependence of the peak position can be described by the interplay between Chol-induced changes in the bilayer thickness and the sound velocity. This concentration dependence disagrees with the coexistence of two separate

phases suggested in the literature for POPC-Chol and DMPC-Chol systems, if the assumed phase domain sizes are much larger than the bilayer thickness. This analysis uses the facts that the assumed coexisting liquid-ordered and solid-ordered domains must have different compositions and that the cooling leads to the coexisting domains of different compositions in the S_0 states. Comparison of the low-temperature Raman data with the phase diagrams suggested for room temperature implies a reasonable scenario that during cooling, there is no partial dissolving or changes in composition for the S_0 phase when the second phase is still liquid.

Concentration dependences of the peak parameters are different for the DOPC-Chol bilayer: both the peak position and the peak width demonstrate the monotonic concentration behavior. This difference with the DMPC and POPC bilayers may be attributed to a particularity in disturbance of the DOPC

lateral structure by Chol molecules and deserves further investigation.

For bilayers of fully saturated DMPC, we found a Chol-induced increase of monolayer eigenmode intensity, which is rather small in the absence of Chol. This evidences that Chol addition results here in an efficient monolayer decoupling.

ACKNOWLEDGMENTS

This work was supported by RFBR Grant No. 16-03-00664 and by State Assignment No. AAAA-A17-117052410033-9. S.A.D. acknowledges support from RSF, Grant No. 15-15-00021. Some part of the experiments was performed in the multiple-access center “High-Resolution Spectroscopy of Gases and Condensed Matters” in IA&E SBRAS (Novosibirsk, Russia).

-
- [1] Y. H. Chan and S. G. Boxer, *Curr. Opin. Chem. Biol.* **11**, 581 (2007).
- [2] S. L. Veatch and S. L. Keller, *Biochim. Biophys. Acta* **1746**, 172 (2005).
- [3] D. Marsh, *Biochim. Biophys. Acta* **1788**, 2114 (2009).
- [4] M. A. Alonso and J. Millán, *J. Cell Sci.* **114**, 3957 (2001).
- [5] D. A. Brown and E. London, *Annu. Rev. Cell Dev. Biol.* **14**, 111 (1998).
- [6] P. M. Winkler, R. Regmi, V. Flauraud, J. Brugger, H. Rigneault, J. Wenger, and M. F. Garcia-Parajo, *J. Phys. Chem. Lett.* **9**, 110 (2017).
- [7] A. S. Klymchenko and R. Kreder, *Chem. Biol.* **21**, 97 (2014).
- [8] J. Juhasz, F. J. Sharom, and J. H. Davis, *Biochim. Biophys. Acta* **1788**, 2541 (2009).
- [9] B. M. Castro, L. C. Silva, A. Fedorov, R. F. de Almeida, and M. Prieto, *J. Biol. Chem.* **284**, 22978 (2009).
- [10] J. Zhao, J. Wu, H. Shao, F. Kong, N. Jain, G. Hunt, and G. Feigenson, *Biochim. Biophys. Acta* **1768**, 2777 (2007).
- [11] T. Yasuda, H. Tsuchikawa, M. Murata, and N. Matsumori, *Biophys. J.* **108**, 2502 (2015).
- [12] J. L. Thewalt and M. Bloom, *Biophys. J.* **63**, 1176 (1992).
- [13] I. V. Ionova, V. A. Livshits, and D. Marsh, *Biophys. J.* **102**, 1856 (2012).
- [14] W. D. Bennett and D. P. Tieleman, *Biochim. Biophys. Acta* **1828**, 1765 (2013).
- [15] H. J. Risselada and S. J. Marrink, *Proc. Natl. Acad. Sci. USA* **105**, 17367 (2008).
- [16] S. Munro, *Cell* **115**, 377 (2003).
- [17] S. Mayor and M. Rao, *Traffic* **5**, 231 (2004).
- [18] L. J. Pike, *J. Lipid Res.* **47**, 1597 (2006).
- [19] J. F. Hancock, *Nat. Rev. Mol. Cell Biol.* **7**, 456 (2006).
- [20] D. Marguet, P. F. Lenne, H. Rigneault, and H. He, *EMBO J.* **25**, 3446 (2006).
- [21] K. Jacobson, O. G. Mouritsen, and R. G. W. Anderson, *Nat. Cell Biol.* **9**, 7 (2007).
- [22] E. Klotzsch and G. J. Schütz, *Philos. Trans. R. Soc. B Biol. Sci.* **368**, 20120033 (2013).
- [23] D. Marsh, *Biochim. Biophys. Acta* **1798**, 688 (2010).
- [24] Q. Waheed, R. Tjörnhammar, and O. Edholm, *Biophys. J.* **103**, 2125 (2012).
- [25] N. V. Surovtsev, A. A. Dmitriev, and S. A. Dzuba, *Phys Rev E* **95**, 032412 (2017).
- [26] P. F. de Almeida, W. L. Vaz, and T. E. Thompson, *Biochemistry* **31**, 6739 (1992).
- [27] R. F. de Almeida, A. Fedorov, and M. Prieto, *Biophys. J.* **85**, 2406 (2003).
- [28] N. V. Surovtsev, *Optoelectron., Instrum. Data Process.* **53**, 250 (2017).
- [29] S. V. Adichtchev, V. R. Belosludov, A. V. Ildyakov, V. K. Malinovsky, A. Yu. Manakov, O. S. Subbotin, and N. V. Surovtsev, *J. Phys. Chem. B* **117**, 10686 (2013).
- [30] B. P. Gaber and W. L. Peticolas, *Biochim. Biophys. Acta* **465**, 260 (1977).
- [31] J.-P. LePessant, L. Powers, and P. S. Pershan, *Proc. Natl. Acad. Sci. USA* **75**, 1792 (1978).
- [32] N. V. Surovtsev and S. A. Dzuba, *J. Phys. Chem. B* **113**, 15558 (2009).
- [33] C. T. Boughter, V. Monje-Galvan, W. Im, and J. B. Klauda, *J. Phys. Chem. B* **120**, 11761 (2016).
- [34] A. Hodzic, P. Zoumpoulakis, G. Pabst, T. Mavromoustakos, and M. Rappolt, *Phys. Chem. Chem. Phys.* **14**, 4780 (2012).
- [35] C. E. Miller, J. Majewski, E. B. Watkins, D. J. Mulder, T. Gog, and T. L. Kuhl, *Phys. Rev. Lett.* **100**, 058103 (2008).
- [36] D. Marsh, *Chem. Phys. Lipids* **165**, 59 (2012).
- [37] B. R. Copeland and H. M. McConnell, *Biochim. Biophys. Acta* **599**, 95 (1980).
- [38] D. J. Recktenwald and H. M. McConnell, *Biochemistry* **20**, 4505 (1981).
- [39] C. R. Mateo, A. U. Acuna, and J.-C. Brochon, *Biophys. J.* **68**, 978 (1995).